

Facile Synthesis of Single Crystal Vanadium Disulfide Nanosheets by Chemical Vapor Deposition for Efficient Hydrogen Evolution Reaction

Jiangtan Yuan, Jingjie Wu, Will J. Hardy, Philip Loya, Minhan Lou, Yingchao Yang, Sina Najmaei, Menglei Jiang, Fan Qin, Kunttal Keyshar, Heng Ji, Weilu Gao, Jiming Bao, Junichiro Kono, Douglas Natelson, Pulickel M. Ajayan, and Jun Lou*

Transition metal dichalcogenides (TMDs) are a class of layered materials with one layer of metal atoms sandwiched between two layers of chalcogen atoms as the monolayer building block.^[1] Bulk TMDs have been extensively studied since 1960s in diverse research areas such as lubrication,^[2] batteries,^[3] charge density wave materials,^[4] and superconductivity,^[5] to name a few. Recently, there is a renewed interest in these materials thanks to the emergence of exciting physics in their 2D forms.^[6,7] Among 2D TMDs, a semiconducting subset of TMDs, where the transition metal is typically Mo or W and the chalcogen atom is S or Se, has received the greatest attention due to their promise in potential electronic^[8] and optoelectronic^[9] applications.

Vanadium disulfide (VS_2) is a typical metallic member of TMDs family without a bandgap in its electronic structure, different from semiconducting MoS_2 or WS_2 .^[10] This metallic behavior has already shown its potential in applications such as supercapacitors^[11] and moisture sensors.^[12] This material also shows promise of having ferromagnetic properties at the 2D limit.^[10,13] More importantly, metallic 2D TMDs are an

indispensable component for building the much-sought in-plane or vertical heterostructures using 2D building blocks, ideally with different electronic properties (i.e., metals, semiconductors, and insulators).^[7,14]

Recent experimental and theoretical progress also suggests that TMDs nanoparticles or nanosheets are inexpensive and earth abundant alternatives to platinum as electrocatalysts for the hydrogen evolution reaction (HER), a critical reaction to generate hydrogen by electrochemical reduction of water. Unlike 2H- MoS_2 and 2H- WS_2 where the HER catalytic activity is thought to originate from the metallic edges,^[15–18] metallic 1T- MoS_2 and 1T- WS_2 have shown better HER performance than their semiconducting counterparts.^[15,19] Considering that VS_2 is a metallic TMD, there is hope that it would have superior catalytic performance for HER, which awaits experimental verification.

Therefore, it is highly desirable to prepare VS_2 nanosheets using a facile method. There are very limited publications reporting the synthesis of VS_2 since its first preparation in 1977 by delithiation of $LiVS_2$.^[20] Methods such as chemical vapor transport typically need high pressures and long reaction times.^[21] Very recently, Feng et al. successfully synthesized VS_2 by a hydrothermal method and demonstrated its metallic nature.^[11] However, due to the complex chemical environment in solution, it is still challenging to prepare contamination-free samples by a solution-based method. Having been successfully demonstrated in synthesizing other 2D materials such as graphene^[22] and MoS_2 ,^[23] chemical vapor deposition (CVD) has the advantage that it can synthesize contamination-free and high crystalline quality samples with potential for scale-up.^[24] However, there has been no report of CVD synthesis of VS_2 so far.

Here, we report a facile CVD method to synthesize VS_2 single crystal nanosheets. The hexagonal 1T crystalline structures of VS_2 were determined using X-ray diffraction (XRD) and transmission electron microscopy (TEM). With the availability of single crystals, the Raman spectrum of VS_2 was also obtained for the first time. The metallic nature of VS_2 single crystals was confirmed by variable-temperature transport measurements and photoluminescence (PL) spectroscopy. We then investigated the electrocatalytic HER activities of the 1T- VS_2 , which showed extremely low overpotential (-68 meV) at the specific 10 mA cm^{-2} , small Tafel slopes (≈ 34 mV decade⁻¹), and high stability.

J. Yuan, Dr. J. Wu, Dr. P. Loya, Dr. Y. Yang,
Dr. S. Najmaei, M. Jiang, K. Keyshar,
Prof. P. M. Ajayan, Prof. J. Lou
Department of Materials Science and NanoEngineering
Rice University
Houston, TX 77005, USA
E-mail: jlou@rice.edu



W. J. Hardy, H. Ji, Prof. D. Natelson
Department of Physics and Astronomy
Rice University
Houston, TX 77005, USA

M. Lou, W. Gao, Prof. J. Kono
Department of Electrical and Computer Engineering
Rice University
Houston, TX 77005, USA

F. Qin, Prof. J. Bao
Department of Electrical and Computer Engineering
University of Houston
Houston, TX 77204, USA

Prof. J. Bao
Institute of Fundamental and Frontier Sciences
University of Electronic Science and Technology of China
Chengdu 610054, China

DOI: 10.1002/adma.201502075

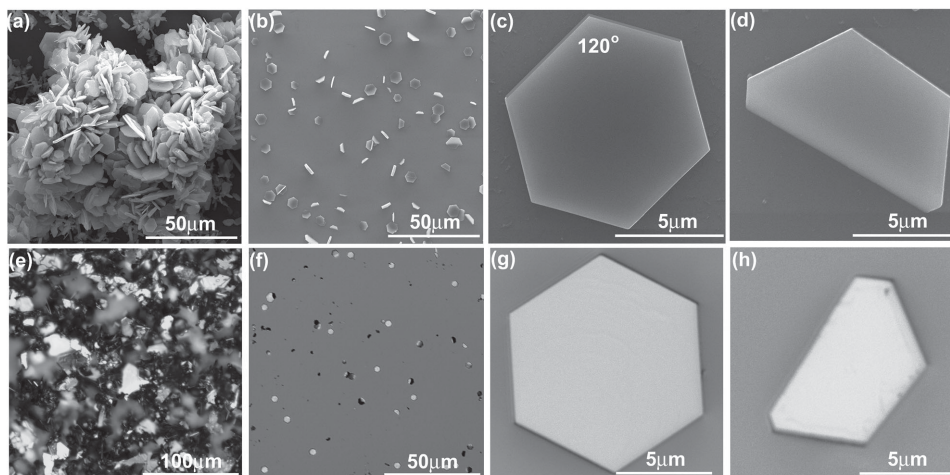


Figure 1. a) Scanning electron microscope (SEM) images of VS_2 nanosheets with different orientations, b) more aligned nanosheets mostly parallel to the substrate, and c) dominant hexagon and d) nearly “half-hexagon” shape for individual crystal. e–h) Corresponding optical images of VS_2 crystals.

The morphology of CVD grown VS_2 crystals is shown in **Figure 1**. At the suitable growth temperature (see details in the Experimental Section), we were able to synthesize large amounts of nanosheets with different orientations of the substrates, as shown in **Figure 1a**. By tuning the amount of precursors, more aligned nanosheets mostly parallel to the substrate are found (**Figure 1b**). Hexagon and nearly “half-hexagon” are the dominant shapes of VS_2 crystals (**Figure 1c,d**), implying the single crystalline nature of the samples. **Figure 1e–h** shows the corresponding optical images of these crystals.

XRD and TEM were performed to determine the crystalline structure of the synthesized VS_2 . **Figure 2a** shows the XRD spectra of a bare SiO_2/Si substrate (top line) and VS_2 nanosheets on substrate having different orientations (middle line). By subtracting the peaks from SiO_2/Si substrate, we can clearly identify the three main diffraction peaks corresponding to (001), (011), and (012) from VS_2 crystals. These peaks match with the PDF database (#01-089-1640) and are in agreement with literature reporting XRD data on VS_2 synthesized using the hydrothermal method,^[11,12] indicating the successful preparation of 1T- VS_2 single crystals by CVD. It is interesting to

note that the XRD spectrum of nanosheets mostly parallel to the substrate (**Figure 1b**) only shows (001) peak in **Figure 2a** (bottom line), suggesting an out-of-plane (001) orientation for the synthesized VS_2 nanosheets. High-resolution TEM images and corresponding electron diffraction patterns along the c -axis (the out-of-plane axis) of a nanosheet were also obtained (**Figure 2b**). From the high-resolution TEM image, the atomic spacing is around 3.2 Å, which matches the lattice parameter of VS_2 ($a = 3.182$ Å, $c = 5.948$ Å).^[11,20,21] The inset of **Figure 2b** shows the selected area electron diffraction pattern of VS_2 crystals. The well-defined hexagonal pattern indicates the hexagonal structure of VS_2 nanosheets basal planes. Only one set of spots was found in the diffraction patterns taken at multiple randomly selected locations, confirming the single crystalline nature.

With the availability of single crystalline VS_2 nanosheets, we are able to study the Raman spectrum of VS_2 as shown in **Figure 3**. We tuned the laser intensities from 0.25 to 25 mW in an attempt to find detectable Raman signal while not damaging the sample by laser irradiation. Overall, the Raman signal of VS_2 is weak, which is similar to other group V metal sulfides (i.e., NbS_2 , TaS_2).^[25,26] At laser intensities lower than 1.25 mW,

there were no noticeable peaks in the spectrum. When the intensity was increased to 2.5 mW, a peak centered around 330 cm^{-1} and a broad peak at about 150 cm^{-1} emerges. At an intensity of 12.5 mW, three main peaks are clearly observed. By comparing with the Raman peaks of TaS_2 ^[26] and NbS_2 ^[25] which have similar crystalline structures with VS_2 , we tentatively assign the peak centered at 330 cm^{-1} to the A_1 out-of-plane vibration mode, the peak centered around 260 cm^{-1} to the E_2 in-plane vibration mode, and the broad peak at about 150 cm^{-1} to a two-phonon process mode. To the best of our knowledge, this is the first time that the Raman spectrum of VS_2 has been reported. Further increasing the laser intensity to 25 mW, the spectrum becomes very different from that at 12.5 mW.

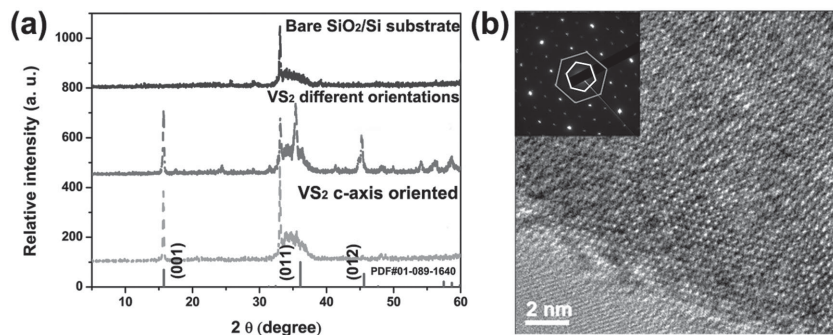


Figure 2. a) XRD patterns of bare SiO_2/Si substrate (top line), VS_2 nanosheets with different orientations, and VS_2 nanosheets mostly parallel to substrates. b) HRTEM image along the c -axis (the out-of-plane axis) of a nanosheet. The atomic spacing is 3.2 Å. Inset is the corresponding electron diffraction pattern. The well-defined hexagonal pattern indicates the hexagonal structure of VS_2 nanosheet basal planes.

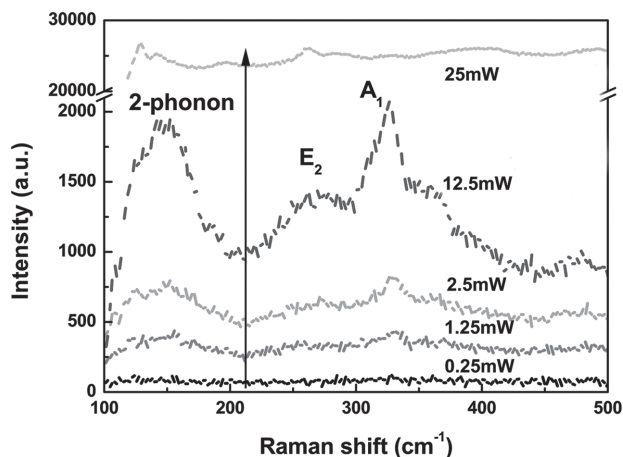


Figure 3. Raman spectrum of VS_2 at different laser intensities. At laser intensities of lower than 2.5 mW, no noticeable peak can be observed. At 12.5 mW, three peaks at 330, 260, and 150 cm^{-1} which correspond to A_1 , E_2 , and two-phonon process modes can be identified. At a laser intensity of 25 mW, the observed Raman spectrum is noticeably different, possibly due to laser-induced chemical damage to the VS_2 .

Both the peak position and peak intensity change dramatically. This spectrum has some features similar to those seen in VO_2 .^[27] At this laser intensity, VS_2 crystals could be burned by the laser and oxidized as we performed Raman spectroscopy at ambient conditions.

The electronic properties of VS_2 were characterized by measuring the resistivity as a function of temperature on their growth substrate. For the particular nanosheet shown in **Figure 4**, the thickness was ≈ 42.5 nm (**Figure 4b**), as determined by atomic force microscopy (AFM) (the thickness distribution of synthesized VS_2 crystals can be found in **Figure S1**, Supporting Information). Metal contacts were defined using electron beam lithography, and made by electron beam evaporation of 5 nm Ti and 45 nm Au, and the subsequent liftoff process. A scanning electron microscopy (SEM) image of the device used for resistivity measurements is shown in

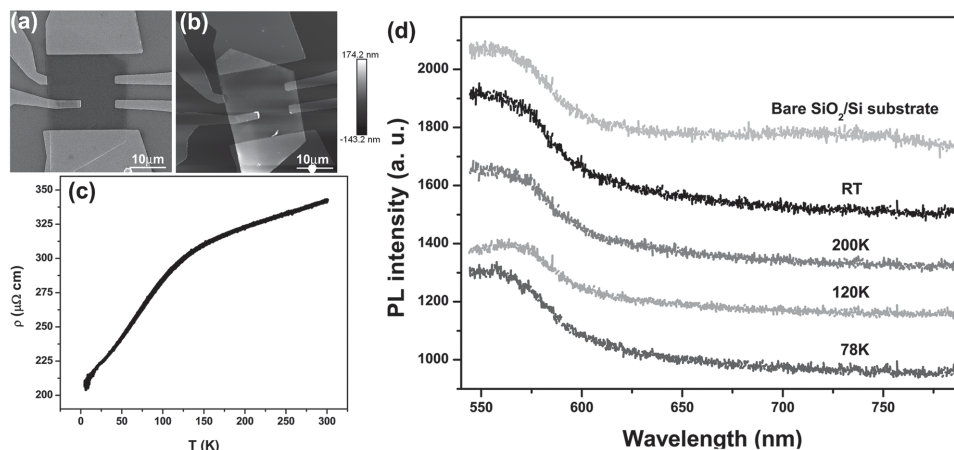


Figure 4. a) SEM image of the device used for resistivity measurements. The upper, down, and right two electrodes were used in four-probe measurement. b) AFM image of the device. The height of the VS_2 crystal is about 42.5 nm. c) Temperature-dependent resistivity curve. As the temperature decreases, the resistivity of VS_2 decreases, showing its metallic behavior. d) PL spectra of VS_2 single crystal at different temperatures. Comparing the signal from the bare growth substrate, there are no noticeable peaks from VS_2 in the wavelength range of 550–780 nm.

Figure 4a. The temperature-dependent resistivity data are shown in **Figure 4c**. The positive slope of the resistivity curve is consistent with metallic conduction throughout the temperature range of 5–300 K. The resistivity of single crystalline VS_2 is ≈ 300 $\mu\Omega$ cm, which is about three orders of magnitude lower than that of samples made by the hydrothermal method,^[11] indicating the high quality of CVD samples. PL spectra at different temperatures were also obtained on VS_2 single crystalline nanosheets (**Figure 4d**). We took the spectra in the wavelength range of 540–780 nm from room temperature down to 78 K. Comparing with the PL from the substrate, there are no observable peaks from VS_2 crystal. This is consistent with the observation of metallic conduction, with no bandgap in the electronic structure of VS_2 , no strong PL peaks would be expected in VS_2 .

After successful preparation of the 1T- VS_2 single crystalline nanosheets, we investigated their electrocatalytic HER activities. VS_2 nanosheets were deposited on a glassy carbon (GC) electrode and subsequently tested in 0.5 M H_2SO_4 electrolyte using a typical three-electrode setup (see the Experimental Section for details). As a comparison, we also measured Pt/C catalyst (20 wt% Pt on Vulcan carbon black) which exhibits high HER catalytic performance with a near zero overpotential for initializing hydrogen evolution. The gas chromatography measurement confirms HER rather than other non-faradaic or corrosion reactions on the VS_2 electrode (**Figure S2**, Supporting Information). The polarization curve (j - E plot) for 1T- VS_2 showed a negligible overpotential for initializing HER similar to the reference Pt electrode (**Figure 5a**). VS_2 also exhibits an extremely low overpotential at 10 mA cm^{-2} , -68 mV, approaching that of -43 mV for Pt. This specific overpotential is much lower than for other TMDs such as 2H-, 1T-MoS₂^[16,19,28] and 2H-, 1T-WSe₂.^[15,18] Moreover, it only requires an overpotential of -0.34 V to achieve 100 mA cm^{-2} for 1T- VS_2 (**Figure S3**, Supporting Information). The high activity of VS_2 probably originates from the high activity of both basal plane and edge sites, both of which have H adsorption free energy approximating to optimal $\Delta G_{\text{H}} = 0$ eV as predicted by the density function theory (DFT) modeling, thus

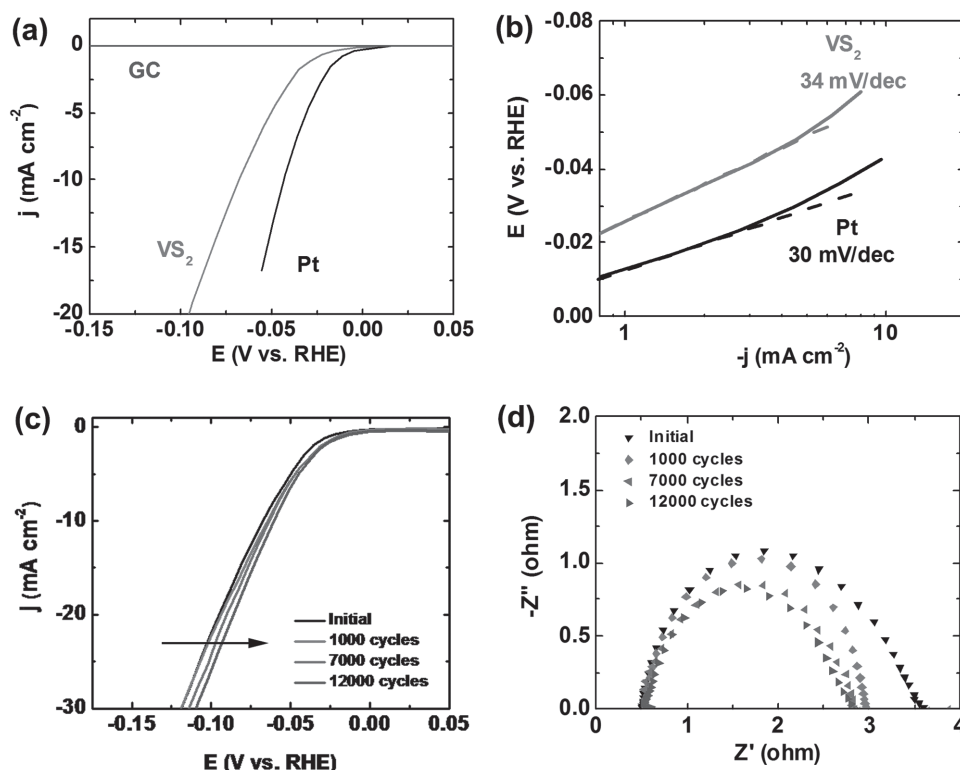


Figure 5. Electrocatalytic performance of 1T-VS₂ crystals. a) Polarization curves after *iR*-correction, b) corresponding Tafel plots, c) polarization curves after various cycles, and d) Nyquist plots showing that 1T-VS₂ maintains excellent catalytic activity after 12,000 cycles of continuous operation.

more active sites are accessible compared to edge activity only for 2H-MoS₂.^[29] In addition, the metallic nature of 1T-VS₂ also contributes to the enhancement of activity by facilitating the electron transfer, which is evidenced by the small charge transfer resistance (Figure 5d). The linear fit of Tafel plots at small overpotential region yields Tafel slopes of ≈ 34 mV decade⁻¹ for 1T-VS₂, slightly higher than ≈ 30 mV decade⁻¹ for Pt (Figure 5b). The surface coverage of H_{ads} for layered TMDs is usually much lower than that for Pt ($\theta_{\text{H}} \approx 1$) at low overpotentials.^[30] Additionally, the DFT calculation shows an activation barrier as high as ≈ 1.5 eV for the recombination step of adsorbed H_{ads} for layered TMDs.^[29] Considering the high catalytic activity at low overpotential, it is highly unlikely that HER on 1T-VS₂ proceeds via the Volmer–Tafel route as for Pt. Thus, HER on 1T-VS₂ most likely proceeds via a Volmer–Heyrovsky mechanism, suggesting that electrochemical desorption is the rate-limiting step. We further tested the durability of 1T-VS₂ for HER. Instead of degradation, it shows a slightly enhanced performance during the continuous potential cycling between 0 and -0.6 V (Figure 5c). The overpotential shifts anodically by ≈ 8 mV at -10 mA cm⁻² after 12,000 cycles. The electrochemical impedance spectroscopy (EIS) measurement shows a smaller initial charge transfer resistance for 1T-VS₂ (3Ω) than the previously reported 1T-MoS₂ (4Ω)^[19] and 1T-WS₂ ($\approx 5 \Omega$).^[31] Interestingly, charge transfer resistance for 1T-VS₂ decreases slightly after potential cycling (Figure 5d), consistent with the increase of performance. The catalytic stability of the 1T-VS₂ was further evaluated by potentiostatic operation. The recorded chronoamperometric (*i-t*) curve at -0.1 V versus RHE (without *iR* compensation) shows gradual increasing of

HER performance within 12 h, consistent with the enhancement of activity during potential cycling (Figure S4, Supporting Information). Overall, 1T-VS₂ is a promising candidate as a non-precious metal catalyst for HER due to its excellent activity and high stability.

In conclusion, we report a facile method to prepare single crystalline VS₂ nanosheets by CVD. We determine the hexagonal 1T crystalline structures of VS₂ using XRD and TEM. The Raman spectrum of VS₂ is obtained for the first time with the availability of single crystals. The metallic nature of VS₂ nanosheets was determined by transport measurement and PL spectroscopy at different temperatures, with a resistivity of about $300 \mu\Omega$ cm. We also investigate the electrocatalytic HER activities of the 1T-VS₂, which shows extremely low overpotential of -68 mV at 10 mA cm⁻², and small Tafel slopes of ≈ 34 mV decade⁻¹ as well as high stability, demonstrating its potential as a candidate non-noble metal catalyst for HER.

Experimental Section

Synthesis of VS₂ by CVD: Vanadium chloride (VCl₃) was used as a precursor in the process of VS₂ preparation. An Al₂O₃ crucible with around 0.5 g of VCl₃ was placed in a quartz tube with diameter of 1 inch at the center of the heating zone of the furnace. An SiO₂/Si substrate was placed on top of the crucible to collect the final product. Sulfur was put in the upstream of the tube. A mixture of N₂ with 10% of H₂ was used as carrier gas at the ambient pressure. The center of the furnace was gradually heated from room temperature to 550 °C in 25 min at a rate of ≈ 20 °C min⁻¹. After 10 min at this temperature, the carrier gas

was changed to pure N₂ and the furnace was naturally cooled down to room temperature.

Characterization Method: The samples were characterized with field-emission scanning electron microscopy (FEI Quanta 400), X-ray diffraction (Rigaku D/Max Ultima II) equipped with Ni-filtered Cu K α radiation (40 kV, 40 mA, $\lambda = 0.15418$ nm), and high-resolution transmission electron microscopy (HRTEM, JEOL JEM-2100 F with a probe size under 0.5 nm, 200 kV). Raman measurements were performed with a micro Raman spectrometer (Renishaw inVia confocal) by focusing the laser radiation centered at 514 nm from an argon-ion laser onto the crystal via a 50 \times objective lens. Variable-temperature transport measurements were performed in a Quantum Design Physical Property Measurement System. The reflectance radiation of PL was collected and analyzed using a grating spectrometer equipped with liquid nitrogen cooled charge coupled device camera.

Electrochemical Measurement: The VS₂ crystals were collected by spin-coating poly (methyl methacrylate) (PMMA) followed by etching SiO₂/Si in 1 M potassium hydroxide (KOH) solution. The float PMMA was cleaned by deionized (DI) water followed dissolving in acetone. The resulted VS₂ was obtained by centrifuging at 5000 rpm for 5 min. The catalyst ink was prepared by mixing the VS₂ crystals, isopropanol, deionized water, and Nafion (0.5 wt%) followed by sonicating for 30 min. 8 μ L catalyst ink was dropped onto a glassy carbon electrode ($A = 0.196$ cm²). The catalyst loading is ≈ 10 μ g cm⁻². Electrochemical measurements were carried out with a three-electrode cell using an Autolab PGSTAT302N potentiostat/galvanostat. A saturated calomel electrode (CH Instruments) was used as the reference electrode with a platinum foil (Alfa Aesar) as the counter electrode. The reference electrode was calibrated for the reversible hydrogen potential using a platinum wire as the working electrode and a platinum foil as the counter electrode in the electrolyte solution saturated with H₂. In 0.5 M H₂SO₄, $E(\text{RHE}) = E(\text{SCE}) + 0.250$ V. Linear sweep voltammetry was performed with a 5 mV s⁻¹ scan rate in 0.5 M H₂SO₄ electrolyte de-aerated with Ar. The potential cycling was performed between 0 and -0.6 V versus RHE at 100 mV s⁻¹. The iR drop was compensated by measuring the electrochemical impedance spectroscopy at -0.2 V versus RHE from 100 K to 0.1 Hz with amplitude of 5 mV. The production of gas in the reactor was taken by a gas-tight syringe and ejected into a gas chromatography (Series 350, Thermal conductivity detector, GOW-MAC Instrument company) to measure the H₂/O₂ molar ratio.

Supporting Information

Supporting Information is available from the Wiley Online Library or from the author.

Acknowledgements

J.Y. and J.W. contributed equally to this work. The authors gratefully acknowledge the support from AFOSR (Grant No. FA9550-14-1-0268) and the Welch Foundation (Grant No. C1716). For the electronic transport characterization, W.J.H., H.J., and D.N. acknowledge support through U.S. Department of Energy, Office of Science, Basic Energy Sciences Award No. DE-FG02-06ER46337. J.M.B. acknowledges support from the Robert A. Welch Foundation (E-1728).

Received: April 30, 2015

Revised: July 13, 2015

Published online:

[1] Q. H. Wang, K. Kalantar-Zadeh, A. Kis, J. N. Coleman, M. S. Strano, *Nat. Nanotechnol.* **2012**, *7*, 699.

- [2] J. Martin, C. Donnet, T. Le Mogne, T. Epicier, *Phys. Rev. B* **1993**, *48*, 10583.
- [3] M. S. Whittingham, *Chem. Rev.* **2004**, *104*, 4271.
- [4] J. Wilson, F. Di Salvo, S. Mahajan, *Phys. Rev. Lett.* **1974**, *32*, 882.
- [5] B. Sipoš, A. F. Kusmartseva, A. Akrap, H. Berger, L. Forro, E. Tutis, *Nat. Mater.* **2008**, *7*, 960.
- [6] K. F. Mak, C. Lee, J. Hone, J. Shan, T. F. Heinz, *Phys. Rev. Lett.* **2010**, *105*, 136805.
- [7] A. K. Geim, I. V. Grigorieva, *Nature* **2013**, *499*, 419.
- [8] B. Radisavljevic, A. Radenovic, J. Brivio, V. Giacometti, A. Kis, *Nat. Nanotechnol.* **2011**, *6*, 147.
- [9] F. N. Xia, H. Wang, D. Xiao, M. Dubey, A. Ramasubramaniam, *Nat. Photonics* **2014**, *8*, 899.
- [10] Y. D. Ma, Y. Dai, M. Guo, C. W. Niu, Y. T. Zhu, B. B. Huang, *ACS Nano* **2012**, *6*, 1695.
- [11] J. Feng, X. Sun, C. Wu, L. Peng, C. Lin, S. Hu, J. Yang, Y. Xie, *J. Am. Chem. Soc.* **2011**, *133*, 17832.
- [12] J. Feng, L. Peng, C. Wu, X. Sun, S. Hu, C. Lin, J. Dai, J. Yang, Y. Xie, *Adv. Mater.* **2012**, *24*, 1969.
- [13] C. Ataca, H. Şahin, S. Ciraci, *J. Phys. Chem. C* **2012**, *116*, 8983.
- [14] Z. Liu, L. Ma, G. Shi, W. Zhou, Y. Gong, S. Lei, X. Yang, J. Zhang, J. Yu, K. P. Hackenberg, A. Babakhani, J. C. Idrobo, R. Vajtai, J. Lou, P. M. Ajayan, *Nat. Nanotechnol.* **2013**, *8*, 119.
- [15] D. Voiry, H. Yamaguchi, J. W. Li, R. Silva, D. C. B. Alves, T. Fujita, M. W. Chen, T. Asefa, V. B. Shenoy, G. Eda, M. Chhowalla, *Nat. Mater.* **2013**, *12*, 850.
- [16] T. F. Jaramillo, K. P. Jorgensen, J. Bonde, J. H. Nielsen, S. Horch, I. Chorkendorff, *Science* **2007**, *317*, 100.
- [17] H. I. Karunadasa, E. Montalvo, Y. J. Sun, M. Majda, J. R. Long, C. J. Chang, *Science* **2012**, *335*, 698.
- [18] L. Cheng, W. Huang, Q. Gong, C. Liu, Z. Liu, Y. Li, H. Dai, *Angew. Chem., Int. Ed.* **2014**, *53*, 7860.
- [19] M. A. Lukowski, A. S. Daniel, F. Meng, A. Forticaux, L. Li, S. Jin, *J. Am. Chem. Soc.* **2013**, *135*, 10274.
- [20] D. W. Murphy, C. Cros, F. J. Disalvo, J. V. Waszczak, *Inorg. Chem.* **1977**, *16*, 3027.
- [21] M. Mulazzi, A. Chainani, N. Katayama, R. Eguchi, M. Matsunami, H. Ohashi, Y. Senba, M. Nohara, M. Uchida, H. Takagi, S. Shin, *Phys. Rev. B* **2010**, *82*, 075130.
- [22] a) K. S. Novoselov, V. I. Fal'ko, L. Colombo, P. R. Gellert, M. G. Schwab, K. Kim, *Nature* **2012**, *490*, 192; b) J. Yuan, L. P. Ma, S. Pei, J. Du, Y. Su, W. Ren, H. M. Cheng, *ACS Nano* **2013**, *7*, 4233.
- [23] a) S. Najmaei, Z. Liu, W. Zhou, X. Zou, G. Shi, S. Lei, B. I. Yakobson, J. C. Idrobo, P. M. Ajayan, J. Lou, *Nat. Mater.* **2013**, *12*, 754; b) Y. Zhan, Z. Liu, S. Najmaei, P. M. Ajayan, J. Lou, *Small* **2012**, *8*, 966.
- [24] S. Bae, H. Kim, Y. Lee, X. Xu, J. S. Park, Y. Zheng, J. Balakrishnan, T. Lei, H. R. Kim, Y. I. Song, Y. J. Kim, K. S. Kim, B. Ozyilmaz, J. H. Ahn, B. H. Hong, S. Iijima, *Nat. Nanotechnol.* **2010**, *5*, 574.
- [25] W. G. McMullan, J. C. Irwin, *Solid State Commun.* **1983**, *45*, 557.
- [26] S. Sugai, K. Murase, S. Uchida, S. Tanaka, *Solid State Commun.* **1981**, *40*, 399.
- [27] C. Cheng, K. Liu, B. Xiang, J. Suh, J. Wu, *Appl. Phys. Lett.* **2012**, *100*, 103111.
- [28] J. Shi, D. Ma, G. F. Han, Y. Zhang, Q. Ji, T. Gao, J. Sun, X. Song, C. Li, Y. Zhang, X. Y. Lang, Y. Zhang, Z. Liu, *ACS Nano* **2014**, *8*, 10196.
- [29] C. Tsai, K. Chan, J. K. Nørskov, F. Abild-Pedersen, *Surf. Sci.* **2015**, DOI: 10.1016/j.susc.2015.01.019.
- [30] B. Hinnemann, P. G. Moses, J. Bonde, K. P. Jørgensen, J. H. Nielsen, S. Horch, I. Chorkendorff, J. K. Nørskov, *J. Am. Chem. Soc.* **2005**, *127*, 5308.
- [31] M. A. Lukowski, A. S. Daniel, C. R. English, F. Meng, A. Forticaux, R. J. Hamers, S. Jin, *Energy Environ. Sci.* **2014**, *7*, 2608.